

Transport of cosmic rays in the nearby starburst galaxy NGC 253^{*}

V. Heesen^{1,3,**}, R. Beck², M. Krause², and R.-J. Dettmar³

¹ Centre for Astrophysics Research, University of Hertfordshire, Hatfield AL10 9AB, UK

² Max-Planck-Institut für Radioastronomie, Auf dem Hügel 69, 53121 Bonn, Germany

³ Astronomisches Institut der Ruhr-Universität Bochum, Universitätsstr. 150, 44780 Bochum, Germany

Received September 2009

Published online later

Key words galaxies: individual: NGC 253 - Cosmic rays - methods: observational - galaxies: magnetic fields - galaxies: halos - galaxies: ISM

Radio halos require the coexistence of extra-planar cosmic rays and magnetic fields. Because cosmic rays are injected and accelerated by processes related to star formation in the disk, they have to be transported from the disk into the halo. A vertical large-scale magnetic field can significantly enhance this transport.

We observed NGC 253 using radio continuum polarimetry with the Effelsberg and VLA telescopes.

The radio halo of NGC 253 has a dumbbell shape with the smallest vertical extension near the center. With an estimate for the electron lifetime, we measured the cosmic-ray bulk speed as $300 \pm 30 \text{ km s}^{-1}$ which is constant over the extent of the disk. This shows the presence of a “disk wind” in NGC 253. We propose that the large-scale magnetic field is the superposition of a disk (r, ϕ) and halo (r, z) component. The disk field is an inward-pointing spiral with even parity. The conical (even) halo field appears in projection as an X-shaped structure, as observed in other edge-on galaxies.

Interaction by compression in the walls of the superbubbles may explain the observed alignment between the halo field and the lobes of hot $\text{H}\alpha$ - and soft X-ray emitting gas. The disk wind is a good candidate for the transport of small-scale helical fields, required for efficient dynamo action, and as a source for the neutral hydrogen observed in the halo.

© 2009 WILEY-VCH Verlag GmbH & Co. KGaA, Weinheim

1 Introduction

Gaseous halos are a common property of star-forming galaxies (Dettmar 1992). How galactic halos are formed is still under debate. One scenario is that star formation in the disk drives an outflow by releasing hot gas and cosmic rays into the interstellar medium. Their combined pressure can drive the outflow against the gravitational pull of the stellar disk. Cosmic rays are particularly well suited because their adiabatic index of $\Gamma = 4/3$ results in a larger pressure scale-height than that of the hot gas ($\Gamma = 5/3$). Moreover, cosmic rays do not lose their energy fast by radiation losses, so that they are able to contribute a significant pressure even far away from the disk. Breitschwerdt et al. (1991) showed that the cosmic-ray pressure is able to accelerate the flow in the halo, so that it can escape from the gravitational potential as a galactic wind. A galactic wind, hybridly driven by the cosmic-ray and thermal gas, may be present in the Milky Way (Everett et al. 2008).

The structure of the large-scale magnetic field significantly influences the cosmic-ray transport. A vertical field enhances the transport from the disk into the halo, because

the diffusion coefficient along the field lines is larger than perpendicular to them. Vertical magnetic field components have indeed been found in the halos of several nearby edge-on galaxies. They all show an X-shaped field pattern like in NGC 5775 (Tüllmann et al. 2000) and in NGC 891 (Krause 2007). How these fields are formed is still under debate. The geometry of the flow is shaped by the gravitational potential and the pressure balance in the halo, so that it can have a radial structure (Fichtner et al. 1991). The magnetic field lines may trace the direction of the flow which has vertical and radial components, so that in projection it forms an X-shape. Hydro simulations of disk galaxies with star formation show also an X-shaped gas flow (Dalla Vecchia & Schaye 2008).

Another question is how large-scale magnetic fields are generated in galaxies. The α - Ω dynamo is among the favorite explanations but it remains to be clarified how it works in presence of a galactic wind. One requirement is that small-scale helical fields are expelled from the galaxy (Sur et al. 2007). Parker (1992) pointed out the importance of cosmic rays to drive a fast dynamo where the magnetic field amplification is enhanced by magnetic reconnection. Global MHD simulations of cosmic-ray driven galactic dynamos show that field amplification is possible and that the X-shaped structure can be reproduced (Hanasz et al. 2009a,b).

NGC 253 is a nearby starburst galaxy which allows us to study its structure in high detail ($D = 3.94 \text{ Mpc}$, $30'' = 600 \text{ pc}$). It has one of the brightest radio halos known, but

^{*} This work is based on observations with the Effelsberg 100m and the VLA radio telescopes. The Effelsberg telescope is operated by the Max-Planck Institut für Radioastronomie (MPIfR). The VLA (Very Large Array) is operated by the NRAO (National Radio Astronomy Observatory).

^{**} Corresponding author: e-mail: v.heesen@herts.ac.uk

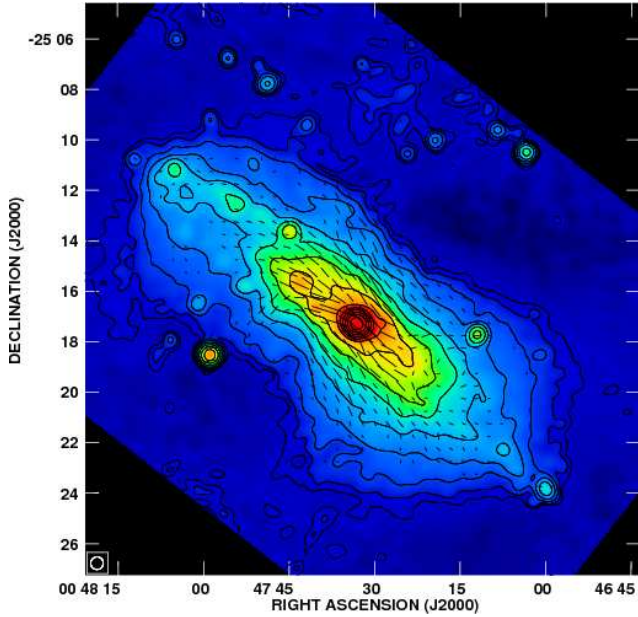


Fig. 1 Total power radio continuum at $\lambda 6.2$ cm obtained from the combined VLA + Effelsberg observations, smoothed to $30''$ resolution. Contours are at 3, 6, 12, 24, 48, 96, 192, 384, 768, 1536, 3077, 6144, 12288, and $24576 \times$ the rms noise of $30 \mu\text{Jy}/\text{beam}$. The overlaid vectors indicate the orientation of the Faraday-corrected ordered magnetic field. A vector length of $1''$ is equivalent to $12.5 \mu\text{Jy}/\text{beam}$ polarized intensity.

so far a vertical magnetic field could not be found (Beck et al. 1994). It has a prominent gaseous halo that is visible in soft X-ray, $\text{H}\alpha$, and H I emission (Bauer et al. 2008; Hoopes et al. 1996; Boomsma et al. 2005) which makes it one of the best candidates besides M 82 for a superwind (Heckman et al. 2000).

2 Observations

We observed NGC 253 in the radio continuum polarimetry mode using the Effelsberg 100m single-dish telescope and the VLA interferometer in D-configuration. A deep VLA mosaic at $\lambda 6.2$ cm was combined with 100-m Effelsberg observations in order to fill-in the missing zero-spacing flux. Moreover, we observed with the Effelsberg telescope at $\lambda 3.6$ cm and used VLA maps from the archive at $\lambda\lambda 20$ cm and 90 cm. Details of the observations and data reduction can be found in Heesen (2008) and Heesen et al. (2008; 2009).

3 Cosmic-ray transport

Cosmic-ray electrons undergo several energy losses, among them loss due to synchrotron radiation is dominant. The synchrotron energy loss depends on the electron energy and the magnetic field strength as $dE/dt \propto E^2 B^2$. Electrons with higher energies have a shorter lifetimes, which causes a steepening of the electron spectral index with time, known

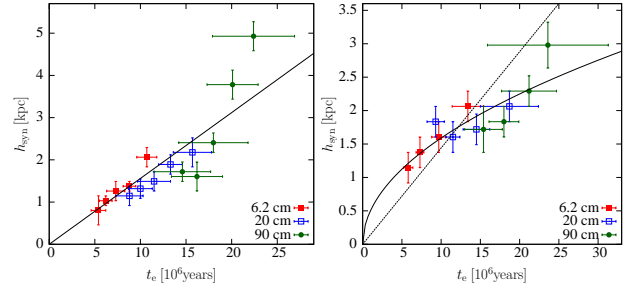


Fig. 2 Scaleheight h_{syn} of the thick radio disk as a function of the electron lifetime t_e in the northeastern halo (left) and in the southwestern halo (right). The linear fit is the theoretical expectation for a convective cosmic-ray transport with a constant bulk speed. The fit $h_{\text{syn}} \propto \sqrt{t_e}$ is the theoretical expectation for a diffusive cosmic-ray transport.

as electron aging (e.g. Longair 2008). The electron spectral index γ is related to the radio spectral index by $\alpha = (\gamma - 1)/2$. When electrons are injected and accelerated in the disk, they have a flat spectral index of $\gamma \simeq 2$. In the halo, the electron population is aged and the spectral index is steep. We now use the electron lifetime to measure the cosmic-ray bulk speed.

In Fig. 1 we present the distribution of the total power emission at $\lambda 6.2$ cm at a resolution of $30''$ together with the orientation of the ordered magnetic field.¹ Note the dumbbell-shaped halo that has its smallest vertical extent near the center of the galaxy. The vertical profiles of the emission can be characterized by a two-component exponential distribution, which is the superposition of a thin and a thick radio disk. The thin radio disk corresponds to the star-forming disk and has a scaleheight of 0.4 kpc. The thick radio disk corresponds to the electrons in the halo with a mean scaleheight of 1.7 kpc. The scaleheight is a useful measure to characterize the radio halo, because it is almost independent of the sensitivity and resolution of the observations. We found that the scaleheight depends on the galactocentric radius with a minimum near the center whereas it is larger further out.

We determined the equipartition magnetic field strengths using the revised formula by Beck & Krause (2005) with a proton to electron ratio of $K = 100$. The magnetic field strength in the disk is between $7 \mu\text{G}$ and $18 \mu\text{G}$. The magnetic field strength is highest near the center of the galaxy where the electron lifetime is smallest. We now define the average cosmic-ray bulk speed as

$$v = \frac{h_e}{t_e}, \quad (1)$$

where h_e is the electron scaleheight ($h_e = 2h_{\text{syn}}$, assuming equipartition) and t_e is the electron lifetime. In Fig. 2 the synchrotron scaleheight is shown as a function of the electron lifetime. In the northeastern halo we find a linear dependence between the electron scaleheight and lifetime. This is indicative of convective transport of cosmic rays and

¹ All resolutions are referred to as the half power beam width (HPBW).

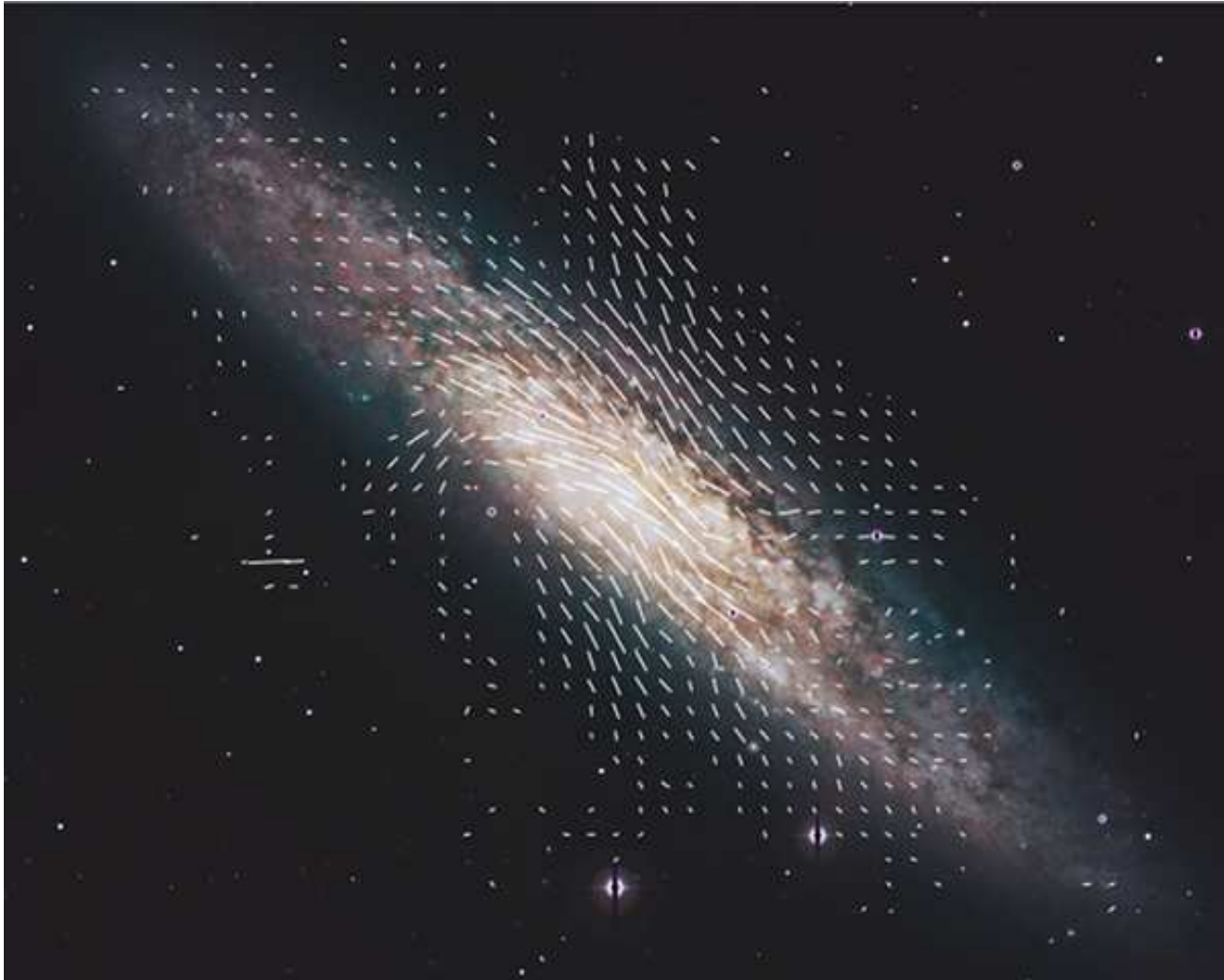


Fig. 3 Orientation of the large-scale magnetic field at $\lambda 6.2$ cm superimposed on an optical image by the ESO widefield imager. Image courtesy of NRAO/AUI.

the magnetic fields. The bulk speed is remarkably constant indicating the presence of a “disk wind” with an average cosmic-ray bulk speed of $300 \pm 30 \text{ km s}^{-1}$. In the southeastern halo the electron scaleheight is proportional to $\sqrt{t_e}$ which is indicative of diffusive cosmic-ray transport. The diffusion coefficient is $\kappa = 2.0 \pm 0.2 \times 10^{29} \text{ cm}^2 \text{ s}^{-2}$.

4 Magnetic field structure

The high linear polarization of the synchrotron emission allows us to measure the orientation of the large-scale magnetic field. Figure 3 shows the magnetic field orientation in NGC 253 superimposed on an optical image. The magnetic field vectors are mainly parallel to the major axis but in some places we find a significant vertical magnetic field component. These are at the locations of the so-called “radio spurs”, where the most prominent one is located east of the nucleus. We propose that the large-scale magnetic field is the superposition of a disk (r, ϕ) and a halo (r, z) component.

In order to test this proposition we created a model for the disk magnetic field using a spiral with a prescribed pitch angle of 25° , similar to the optical pitch angle of 20° (for details of the modeling see Heesen et al. 2009). Spiral fields are observed in the disk of many face-on spiral galaxies like M 51 (Patrikeev et al. 2006). The model shown in Fig. 4 resembles the observed magnetic field well, so that we can presume that the disk magnetic field is dominating. It is not symmetric with respect to the minor axis as the pitch angle shifts the regions with the strongest emission, so that we observe an S-shaped distribution of polarized emission. The vertical field in the radio spurs is strong, so that the emission of the disk is depolarized, otherwise the halo field is hidden by the dominant disk field. This confirms our proposed two-component field structure.

If we subtract the disk magnetic field from the observations we retain the halo magnetic field shown in Fig. 5. It has a prominent X-shaped distribution in polarized intensity and a magnetic field orientation centered on the nucleus. Such magnetic field structures have been observed in sev-

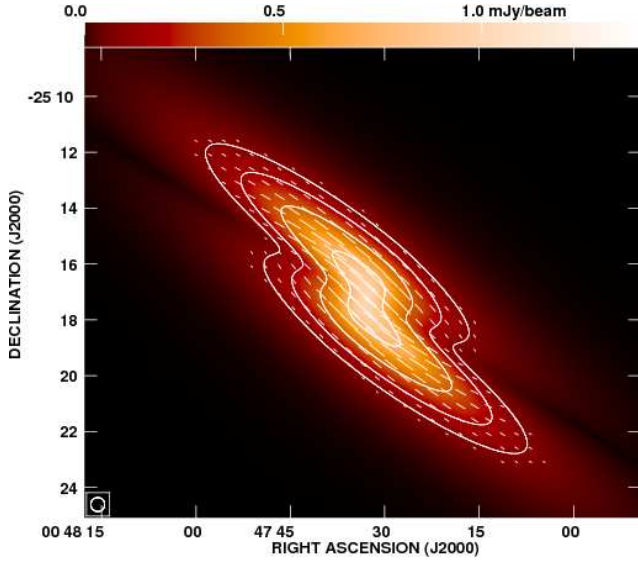


Fig. 4 Modeled polarized intensity at $\lambda 6.2$ cm of the axisymmetric magnetic field (ASS) of the disk at $30''$ resolution. Contours are at $3, 6, 12,$ and $24 \times 30 \mu\text{Jy}/\text{beam}$ of polarized intensity. The vectors indicate the magnetic field orientation where the length of the vectors of $1''$ is equivalent to $12.5 \mu\text{Jy}/\text{beam}$ polarized intensity.

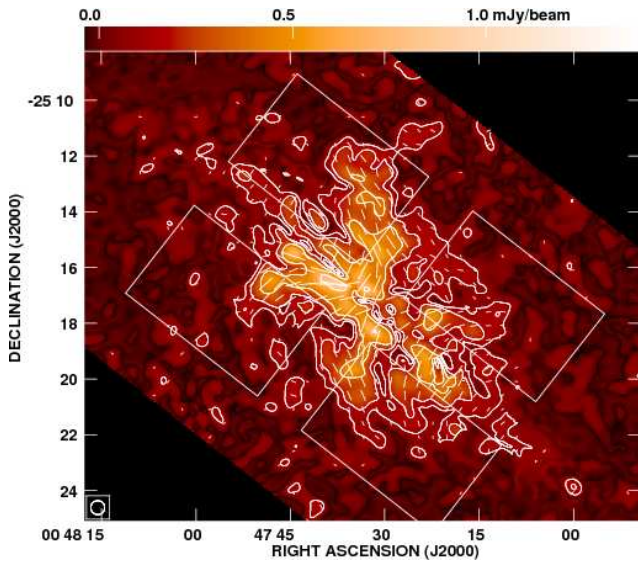


Fig. 5 Polarized intensity at $\lambda 6.2$ cm of the halo magnetic field at $30''$ resolution after subtraction of the disk field model. Contours and vectors are identical to Fig. 4. The boxes for the integration of the orientation angle $\hat{\psi}$ are also shown.

eral nearby edge-on galaxies (Dahlem et al. 1997; Tüllman et al. 2000; Krause et al. 2006; Krause 2007). But this is the first example for a galaxy which is only mildly edge-on ($i = 78.5^\circ$) and is dominated by its disk magnetic field.

The halo magnetic field has an average orientation angle of $\hat{\psi} = 46^\circ \pm 15^\circ$ with respect to the major axis. We propose a conical field with a total opening angle of $\simeq 90^\circ$ that appears as an X-shaped field in projection.

5 Magnetic field direction

So far we have information about the orientation of the large-scale magnetic field in the plane of the sky only. Furthermore, Faraday rotation can tell us the direction and the strength of the magnetic field along the line-of-sight. We determine the Rotation Measure (RM) using the difference of the polarization angles between two wavelengths:

$$\Delta\chi = \text{RM} \cdot (\lambda_1^2 - \lambda_2^2). \quad (2)$$

In Fig. 6 we present the observed RM distribution calculated from the Effelsberg observations at a resolution of $144''$. The northeastern half contains positive RMs (magnetic field pointing to the observer) and the southwestern half negative RMs (pointing away). The sense of the radial rotation velocity is opposite to the RM which is the signature of an inward-pointing magnetic field (Krause & Beck 1998).

Based on the disk magnetic field model (Fig. 4) we created a model RM distribution with a spiral magnetic field pointing inward. In case of a Faraday screen where the polarized emission of a background source passes the electrons and the magnetic field, the RM can be expressed by $RM = \int n_e B_{\parallel} ds$. The azimuthal RM variation of weakly inclined galaxies can then be expressed as a cosine function with a phase shift determined by the pitch angle (Krause et al. 1989). However, NGC 253 is highly inclined (although not edge-on), so that Faraday depolarization effects along the line-of-sight can not be neglected (Sokoloff et al. 1998). Therefore, we use a model to calculate the RM along the line-of-sight which includes Faraday depolarization. The modeled RM distribution shown in Fig. 7 can reproduce the observed asymmetric RM distribution with different amplitudes of the maximum and minimum.

According to our model, the direction of the disk magnetic field is equal on both sides of the galactic midplane. Therefore, the disk field has even parity. In order to study the direction of the halo magnetic field, we made a model for the combined disk and halo field. We tested several possible combinations of field directions in the disk and halo. An even halo field that points away from the disk in the northern and the southern halo fits best to the observations. However, we cannot safely exclude an odd halo field, because we cannot reliably determine the field direction in the northern halo.

6 Galactic wind

In the halo of NGC 253 we find emission from various species of the interstellar medium. Plumes of $\text{H}\alpha$, soft X-ray, and HI emission are extending far into the halo. They are forming shell-like structures with the soft X-ray emission innermost, the HI emission outermost and the $\text{H}\alpha$ in between (Strickland et al. 2002). A fast wind of hot, low-density gas from the nuclear starburst can transport the material into the halo. Such winds are observed in several starburst galaxies and are known as superwinds (Heckman et

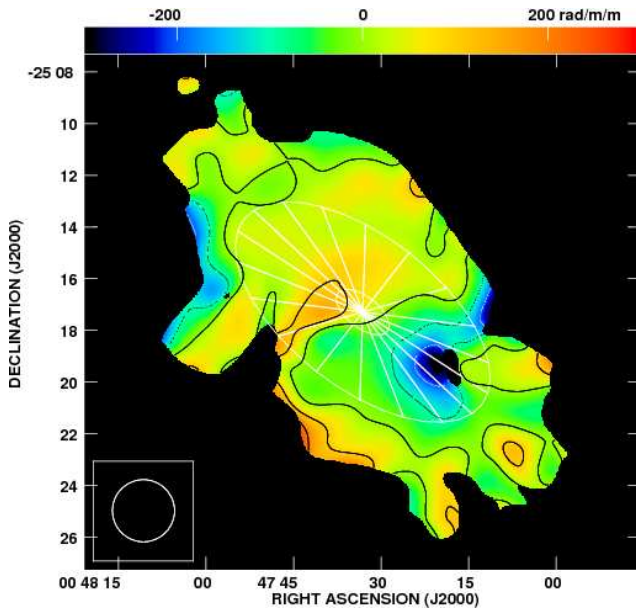


Fig. 6 RM distribution between $\lambda\lambda$ 6.2 cm and 3.6 cm from Efeldsberg observations at $144''$ resolution. Contours are at -200 , -100 , 0 , 100 , and $200 \times 1 \text{ rad m}^{-2}$. The vectors at both wavelengths were clipped below $4\times$ the rms noise level in polarized intensity prior to the combination. The sectors for the azimuthal RM variation are also shown (Heesen et al. 2009).

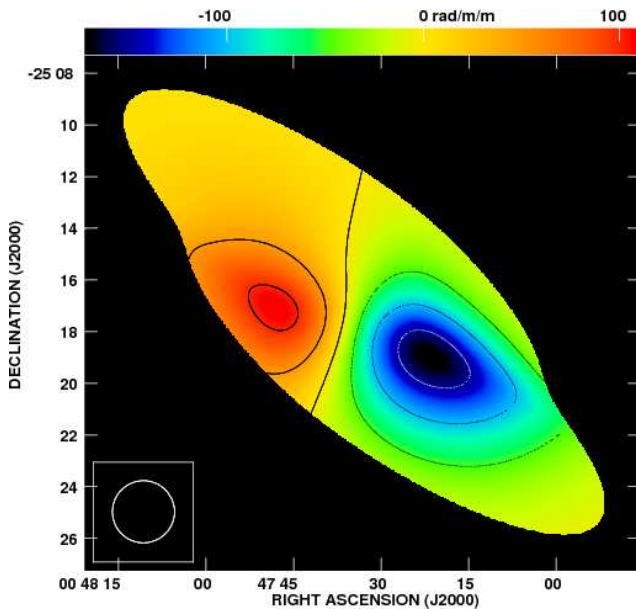


Fig. 7 RM distribution of the axisymmetric spiral (ASS) of the disk magnetic field at $144''$ resolution. Contours are at -150 , -100 , -50 , 0 , 50 , and $100 \times 1 \text{ rad m}^{-2}$. The map was clipped at 0.2 mJy/beam in polarized intensity.

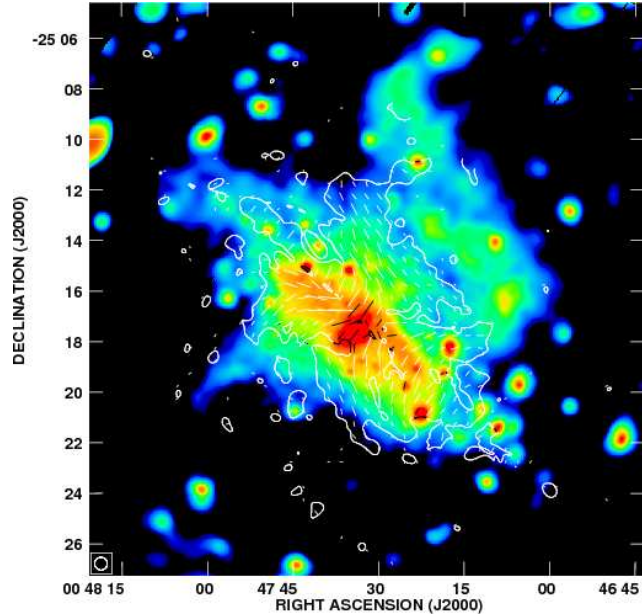


Fig. 8 Halo magnetic field overlaid onto diffuse X-ray emission. The contour is at $3 \times 30 \mu\text{Jy/beam}$ (the rms noise level). A vector length of $1''$ is equivalent to $12.5 \mu\text{Jy/beam}$ polarized intensity. The X-ray map is from XMM-Newton observations in the energy band $0.5 - 1.0 \text{ keV}$ (Bauer et al. 2008).

al. 2000). A second possibility for the transport is the disk wind that is traced by the cosmic rays over the full extent of the disk.

How does the magnetic field relate to the halo structure? In Fig. 8 we show the halo magnetic field as an overlay of soft X-ray emission. The magnetic field is concentrated near the center of the galaxy. Its outer boundary along the major axis is near to the lobes seen in the X-ray emission. Moreover, the orientation of the halo magnetic field is tangential to the lobes. We note that the continuum emission (Fig. 1) does not show any connection to the hot gas but only the polarized emission. The interaction with the superbubble may align and amplify the magnetic field in the shells of the superbubble. Moreover, the magnetic field also shows geometrical limb brightening, because the line-of-sight is perpendicular to the magnetic field lines in the shells. The halo structure together with the magnetic field is shown in Fig. 9.

The field lines in the halo may wind up in a spiral caused by the differential rotation. This field structure is similar to the Parker spiral of the solar magnetic field. On the other hand, if the transport of gas, field, and angular momentum is large, the field lines are expected to corotate far into the halo with no azimuthal component, as observed. The galactic wind can transport angular momentum far better than the superwind in the center at small galactic radii (Zirakashvili et al. 1996). The disk wind is also able to transport the small-scale helical magnetic fields, as requested for efficient dynamo amplification (Sur et al. 2007).

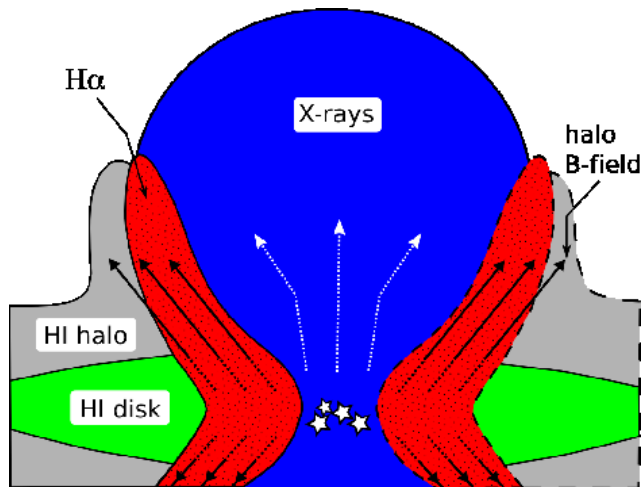


Fig. 9 Halo structure of NGC 253. Reproduced from Boomsma et al. (2005) and extended. The superbubble, filled with soft X-rays emitting gas, expands into the surrounding medium (indicated by dotted lines with arrows). The halo magnetic field is aligned with the walls of the superbubble. Dashed lines denote components that are not (or only weakly) detected in the southwestern half of NGC 253.

7 Conclusions

NGC 253 has a large radio halo. The analysis of the scale-heights of the cosmic-ray electrons and their lifetime shows that this galaxy possesses a disk wind with a cosmic-ray bulk speed of about 300 km s^{-1} . The magnetic field consists of a disk and a halo component. The halo component becomes visible after subtracting the disk and shows a prominent X-shape as known from edge-on galaxies. This is the first X-shaped field in a galaxy which is only mildly edge-on. The disk wind can effectively transport gas from the disk into the halo. The observed magnetic field structure can be explained by the interaction with the superwind by compression in the walls of the superbubble and by limb brightening. Furthermore, the disk wind can transport the small-scale helical fields to ensure efficient dynamo action.

Acknowledgements. The organizers of the Splinter Meeting are thanked for organizing an enjoyable and fruitful meeting.

VH acknowledges the funding by the Graduiertenkolleg GRK 787 and the Sonderforschungsbereich SFB 591 during the course of his PhD. The GRK 787 “Galaxy groups as laboratories for baryonic and dark matter” and the SFB 591 “Universal properties of non-equilibrium plasmas” are funded by the Deutsche Forschungsgemeinschaft (DFG). RJD is supported by DFG in the framework of the research unit FOR 1048.

We thank Michael Bauer for providing the XMM-Newton map and Birgitta Burggraf and Olaf Schmithüsen are thanked for providing the map from the ESO widefield imager.

References

Bauer, M., Pietsch, W., Trinchieri, G., Breitschwerdt, D., Ehle, M., Freyberg, M. J., Read, A. M.: 2008, A&A 489, 1029

- Beck, R., Carilli, C. L., Holdaway, M. A., & Klein, U.: 1994, A&A 292, 409
- Beck, R. & Krause, M.: 2005, AN 326, 414
- Breitschwerdt, D., McKenzie, J. F., & Völk, H. J.: 1991, A&A 245, 79
- Breitschwerdt, D., Dogiel, V. A., Völk, H. J.: 2002, A&A 385, 216
- Boomsma, R., Oosterloo, T., Fraternali, F., van der Hulst J. M., Sancisi, R.: 2005, A&A 431, 65
- Dahlem, M., Petr, M. G., Lehnert, M. D. et al.: 1997, A&A 320, 731
- Dalla Vecchia, C. & Schaye, J.: 2008, MNRAS 387, 1431
- Dettmar, R.-J.: 1992, Fundamentals of Cosmic Physics 15, 143
- Everett, J. E., Zweibel, E. G., Benjamin, R. A. et al.: 2008, ApJ 674, 258
- Fichtner, H., Neusch, W., Fahr, H. J., Schlickeiser, R.: 1991, ApJ 371, 98
- Hanasz, M., Otmianowska-Mazur, K., Kowal, G., Lesch, H.: 2009a, A&A 498, 335
- Hanasz, M., Wółtański, D., Kowalik, K.: 2009b, submitted, e-print arXiv:0907.4891
- Heckman, T. M., Lehnert, M. D., Strickland, D. K., & Armus, L.: 2000, ApJS 129, 493
- Heesen, V.: 2008, PhD thesis, Ruhr-Universität Bochum, Germany
- Heesen, V., Beck, R., Krause, M., & Dettmar, R.-J.: 2008, A&A 494, 563
- Heesen, V., Krause, M., Beck, R., & Dettmar, R.-J.: 2009, A&A accepted, e-print arXiv:0908.2985
- Hoopes, C. G., Walterbos, R. A. M., & Greenwalt, B. E.: 1996, AJ 112, 1429
- Krause, F. & Beck, R.: 1998, A&A 335, 789
- Krause, M.: 2007, Memorie della Societa Astronomica Italiana, Vol. 78, 314
- Krause, M.: 2008, in Magnetic Fields in the Universe II, ed. A. Esquivel, Rev. Mex. Astron. Astrof. (SC), arXiv:astro-ph/0806.2060v2
- Krause, M., Hummel, E., & Beck, R.: 1989, A&A 217, 4
- Krause, M., Wielebinski, R., & Dumke, M.: 2006, A&A 448, 133
- Longair, M.: 2008, High Energy Astrophysics, Volume 2, 2nd edition, Cambridge University Press
- Patrikeev, I., Fletcher, A., Stepanov, R. et al.: 2006, A&A 458, 441
- Sokoloff, D. D., Bykov, A. A., & Shukurov, A. et al.: 1998, MNRAS 299, 189
- Strickland, D. K., Heckman, T. M., & Weaver, K. A. et al.: 2002, ApJ 568, 689
- Sur, S., Shukurov, A. & Subramaniam, K.: 2007, MNRAS 377, 874
- Tüllmann, R., Dettmar, R.-J., & Soida et al.: 2000, A&A 364, L36
- Zirakashvili, V. N., Breitschwerdt, D., Ptuskin, V. S., Völk, H. J.: 1996, A&A 311, 113

